

Defect energies of graphite: Density-functional calculations

L. Li,* S. Reich,[†] and J. Robertson

Department of Engineering, Trumpington Street, University of Cambridge, Cambridge CB2 1PZ, United Kingdom

(Received 8 June 2004; revised manuscript received 24 August 2005; published 30 November 2005)

The energies of point defects in graphite have been calculated from first principles. The various interplane interstitial configurations are found to have a wider range of energies than in some earlier calculations, implying a larger interstitial migration energy than previously expected (>1.5 eV). Interplane interstitials are found to be stabilized by a shear of one graphite plane with respect to its neighbors, as this allows the interstitial to bond to three or four atoms in two planes in the ylid and spiro configurations. The minimum interstitial formation energy in sheared graphite is only 5.3 eV compared to 6.3 eV in perfect graphite. Such interstitials form a strongly bound vacancy-interstitial pair with a formation energy of only 10.2 eV. The formation energy of a single vacancy is 7.6 eV. The formation energy and the activation barrier of the Stone-Wales defect in a single layer of graphite were also calculated.

DOI: [10.1103/PhysRevB.72.184109](https://doi.org/10.1103/PhysRevB.72.184109)

PACS number(s): 61.80.Az, 61.50.Lt, 61.72.Ji, 81.05.Uw

I. INTRODUCTION

Graphite is the most stable phase of carbon and it is used as a catalyst, electrode material, refractory material, and neutron moderator. Graphite consists of layers of three fold coordinated, sp^2 hybridized carbon atoms arranged in an ABAB... stacking sequence. A single atomic layer of graphite or graphene is the structural basis of carbon nanotubes, fullerenes, and related nano-materials, which are presently the subject of intense interest. Nanotubes are of particular interest because of their remarkable properties such as a high stiffness, high electrical conductivity, high current-carrying capacity, and ease of field emission.

There has been considerable experimental work on the intrinsic defects in graphite due to the importance of radiation damage. Until recently, its defects have been less extensively studied at a theoretical level. The simplest intrinsic defects are the vacancy and the interplane and intralayer interstitials. Thrower and Mayer¹ derived the creation and migration energies of the vacancy and the interplane interstitial from experimental data. There have been various calculations of the defects using semiempirical methods.²⁻⁷ Xu *et al.*⁷ used the environmentally dependent tight-binding method to study the various interstitials. However, these calculation methods have an empirical component and may be inaccurate, particularly for the interstitials. The first *ab initio* calculations were the plane-wave pseudopotential calculations of Kaxiras and Pandey.⁸ This work treated only the vacancy and intralayer interstitial, but omitted the equally important interlayer interstitials. The latter defects have only recently been treated by *ab initio* methods by Heggie *et al.*⁹⁻¹¹ These authors found more stable types of interstitial, the spiro and the ylid, in the presence of interlayer shear, and also the possibility of vacancy-interstitial interactions for defects in different layers. These defects have now been observed by electron microscopy between walls in double wall nanotubes.^{12,13} In this paper, we clarify the energies of the various simple and more complex defects using *ab initio* methods.

In addition to these works on defects in bulk graphite, there have been a number of accurate calculations of the

energy of carbon adatoms on graphite, for the purpose of understanding atomic force microscope images of graphite,^{14,15} and also the growth mechanism of carbon nanotubes¹⁶ and nanostructures.¹⁷

Finally, there is the topological rearrangement of bonds in a sp^2 bonded sheet known as the Stone-Wales transformation.¹⁸ It consists of a 90° rotation of a pair of atoms. In graphene, the rearrangement converts a group of four hexagonal rings into a 5-7-7-5 ring cluster by a single bond rotation. This rearrangement is very important in the growth mechanism fullerene molecules such as C_{60} because it is the means for the topological rearrangement of the five fold rings, for example, converting a 5-6-6-5 configuration into a 6-5-5-6 configuration.^{18,19} In nanotubes, the Stone-Wales transformation has become very important²⁰⁻²⁴ because it is believed to be the primary straining mechanism of a nanotube under tensile stress.²⁰

II. COMPUTATIONAL METHOD

Formation energies of defects in graphite were calculated from the total energies of perfect and defected supercells. We performed *ab initio* calculations of the total energies using the CASTEP plane-wave²⁵ and the SIESTA atomic-orbitals²⁶ codes. In this section we first describe the parameters used in the calculations, then the calculation of the formation energies, and how we optimized the supercells with the defect.

A. *Ab initio* calculations

The plane-wave CASTEP calculations used Vanderbilt²⁷ ultrasoft pseudopotentials and k -point sampling by the Monkhorst-Pack scheme. We used a plane-wave cutoff energy of 300 eV. The exchange correlation energy is calculated in the spin-restricted generalized gradient approximation (GGA) of the density functional with the parameterisation of Perdew and Wang (PW91). The GGA is used because of its ability to describe large variations of electron density, noting that graphite has large interstitial regions. Some energies are compared for the local density ap-

proximation (LDA) and GGA, in particular, bulk graphite and the interstitials.

SIESTA calculations were done within GGA and LDA for bulk graphite and the adatoms. For the interstitials, we used SIESTA to perform convergence tests with respect to the size of the supercell in the calculation. This was done within the LDA, because it is computationally less demanding. The carbon core electrons were replaced by Troullier-Martins pseudopotentials;²⁸ valence electrons were described by a double- ζ polarized (DZP) basis set with cutoff radii of 4.5 a.u. for the s and 5.4 a.u. for the p and polarizing d orbitals.²⁹ For the interstitial we also used a double- ζ (DZ) basis (same cutoff radii) to verify the convergence with the size of the supercell, see Sec. IV.

For the calculations of the total energies, we used 3×3 supercells in the in-plane direction of graphite. Cells containing a single sheet of graphite (graphene) and an adatom had 10 Å of vacuum between the layers to prevent interaction between repeated images. The cells contained 19 carbon atoms including the adatom. The interstitials, vacancies, and interstitial-vacancy pairs were calculated in a supercell three layers thick with an *ABA* stacking. In this way, an interstitial atom or a vacancy is placed between two layers *AB* and is always separated by one normal layer before the next cell. The cells contained 54 carbon atoms for the perfect structure plus the added interstitial or minus the removed vacancy atom. We also performed calculations for a $4 \times 4 \times 2$ supercell (*ABAB* stacking) for some selected high-symmetry interstitial positions (129 atoms). Besides being somewhat larger in the *ab* plane, this supercell has the correct stacking sequence of bulk graphite. These calculations were done with SIESTA and the less expensive DZ basis as described above.

B. Formation energies and relaxation

The formation energies E_f were obtained from the total energies of the supercells with a defect,³⁰

$$E_f = E_d - E_{bulk} - n\mu,$$

where E_d is the total energy of the defected supercell and E_{bulk} the total energy of perfect graphite, which we calculated for supercells of the same size as used in the runs with the defects. μ is the chemical potential of carbon, which we took as the total energy of graphite. n gives the number of carbon atoms that were added (n positive) or removed (n negative). Note that configurations with smaller formation energy are more stable (smaller total energy) than configurations with larger E_f .

Calculations of formation energies are difficult to converge, because the total energies of a supercell are typically on the order of 10^3 eV, whereas the formation energies are only some eV. A convergence of the formation energy within 0.1 eV requires, therefore, the total energies to be accurate within 10^{-5} . At the same time large supercells are necessary to have well-separated defects that cannot interact with each other. The combination of the required high accuracy and the large number of atoms make the calculations very demanding. We estimate that the calculated relative formation energies are converged within 0.2 eV. By this we mean two for-

mation energies obtained with the same exchange-correlation functional, pseudopotentials, and plane-wave or local-orbital code. The absolute error in the calculated energies is larger, on the order of 0.5 eV. This estimate is based on recalculating selected structures with better input parameters and the comparison between the formation energies found with CASTEP and SIESTA. The difference between the relative and absolute energies will become more apparent when we discuss the formation energies of adatoms and interstitials in Secs. IV and V. The bond lengths are converged within 0.01 Å unless explicitly stated otherwise. This accuracy was estimated by comparing bond lengths (and angles) obtained with the different *ab initio* methods.

The total energies of the cells with the defects were optimized for the atomic positions until all forces were below 0.05 eV/Å. In the calculations at least one of the corner atoms in the supercell was fixed to its position. For un-sheared graphite all corner atoms were fixed, so that the planes could not move with respect to each other.

The adatom and interstitials were placed into high-symmetry sites, see Secs. IV and V. They were fixed in these places within the *ab* plane and allowed to relax along *c*. With SIESTA we optimized the positions of the adatoms and interstitials along *c* during the conjugate gradient optimisation, i.e., the atoms were allowed to move along the *c* axis. CASTEP does not allow constraining the position along certain directions only. We therefore optimized the position of the adatoms and interstitials manually by performing several runs with different *c* positions for the added atom.

In the calculations for the vacancies all atoms except the corner atoms of the supercell were allowed to find their minimum energy position. During the relaxation of the Stone-Wales defect (5×5 supercell of graphene), the rotated bond and the corner atoms were fixed; the other positions were optimized. We carefully verified the convergence of our systems. The most extensive tests were performed for adatoms and interstitials; the results are described in Secs. IV and V.

III. BULK GRAPHITE

The calculated lattice constants for bulk graphite are shown in Table I. We find an equilibrium in-plane lattice constant of $a_0 = 2.439$ Å using CASTEP and the GGA, slightly less than experiment. The c/a_0 ratio varied between 2.65 and 2.94. Van der Waals interactions as between two layers of graphite are, in general, rather poorly described by density functional theory. In view of this, our *c* axis lattice constants are in reasonable agreement with experiment $c/a_0 = 2.74$; see Table I. A very useful review of calculations of the band structure and structural properties of graphite is given by Boettger.³²

The calculated cohesive energy E_c is 35% larger than experiment using the LDA; see Table I. In many systems, the LDA overestimates the cohesive energy, and this effect is improved by using the GGA. In our calculations this reduced the difference between experiment and theory to 25% in the spin-restricted calculations. An isolated carbon atom, however, is in the triplet state. Thus, the cohesive energy is only given correctly if spin polarized calculations are used for the

TABLE I. Calculated cohesive energy and lattice constants of hexagonal graphite, compared to the calculations by Furthmüller *et al.* (Ref. 25) (using similar pseudopotentials as used for CASTEP in this work) and experiment (Exp.); spin. pol. stands for spin polarized calculation.

	Plane wave, CASTEP			Atomic orbitals, SIESTA		Exp.
	GGA	LDA	Furthmüller	GGA	LDA	
a_0 , Å	2.439	2.439	2.44	2.492	2.466	2.461
c/a	2.94	2.72	2.734	2.81	2.65	2.73
E_c (eV)	-9.42	-10.05	-9.027	-9.1	-9.92	-7.374
E_c , spin pol. (eV)	-8.3	-9.6		-7.74	-8.88	

free atom. Taking this into account we find $E_c = -8.30$ eV using CASTEP and -7.74 eV using SIESTA. GGA and spin polarization thus account for the largest part of the overestimate of the cohesive energy. However, for graphite the GGA leads to a reduction of the interlayer bonding, an overestimate of the c lattice constant (see Table I) and a very low surface energy.³¹ Hence GGA predicts some structural properties of graphite worse than LDA.

IV. ADATOMS ON A SINGLE LAYER

We first consider the energies of a single additional carbon atom on a single layer of graphite, equivalent to an adatom on the graphite surface. There are five high-symmetry positions for an adatom, as shown in Fig. 1. The most important are *A*, the bridge site above the bond center between two layer atoms, *C* above the center of a hexagon of bonds, and *D* directly on top of an atom.

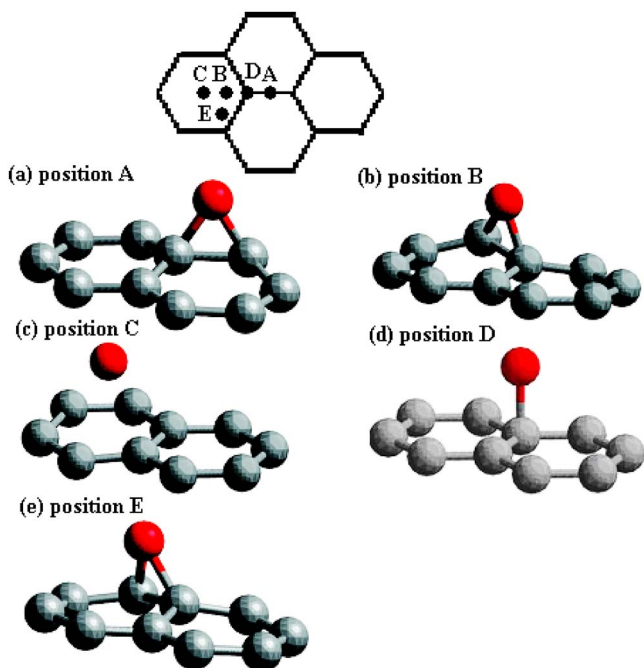


FIG. 1. (Color online) Configuration of an adatom at the various symmetry sites on a single graphene layer (graphene). Light gray atoms are part of graphene; the adatom is dark gray (red). The inset on top shows the high-symmetry sites of a single graphene sheet.

The total energies of the adatom in the five sites are given in Table II. For sites *A*, *B*, *C*, and *D* we compare the CASTEP and SIESTA results. The average difference between the two calculations is 3% (0.2 eV root mean square). We expected such differences, since a fully converged calculation requires a larger basis (higher energy cutoffs and longer basis function) and also a finer sampling in reciprocal space. However, our main interests are the differences in formation energy between the high-symmetry sites. As can be seen from Table II, they are larger than the deviations between CASTEP and SIESTA. In particular, the order of the formation energies is the same in the two *ab initio* codes. We therefore conclude that our *ab initio* formation energies are converged within the accuracy required for this study.

The lowest energy site is found to be the bridge site *A*; see Table II. Here, the adatom is bonded to two layer atoms with a bond length of 1.51 Å, as seen in Fig. 1(a). Meanwhile, the bond between the atoms within the layer weakens a little, increasing its length from 1.41 Å to 1.56 Å. Thus, the adatom is forming two reasonably strong bonds. The next most stable position is *E*. This adatom is similar to site *A*, except that the bond is tilted. This allows the adatom to bond to two atoms with one slightly shorter bond of 1.5 Å and one bond of 1.51 Å [Fig. 1(e)]. The in-plane bond lengthens to 1.55 Å. The next most stable site is *B* [Fig. 1(c)]. At site *B*, the adatom makes a shorter bond of 1.49 Å and a longer bond of 1.65 Å, lengthening the in-plane bond to 1.52 Å.

At the on-top site *D* the adatom bonds directly to only one layer atom if we do not relax the atomic coordinates. We show this configuration in Fig. 1(d); the bond length is 1.55 Å. This position is 1 eV less stable than site *A*. The symmetric on-top position *D* is unstable; relaxing the atomic positions allows the adatom to strain the graphene layer, so that it can form a shorter bond of 1.48 Å to the nearest atom

TABLE II. Calculated formation energies of an adatom at various positions as obtained with CASTEP and SIESTA; compare Fig. 1.

Site	A Bridge	B	C Center	D On top	E	Isolated (triplet)
GGA, CASTEP						
E_f (eV)	6.6	6.9	8.5	7.2	6.8	8.3
GGA, DZP, SIESTA						
E_f , (eV)	6.3	6.8	8.2	7.2		7.7

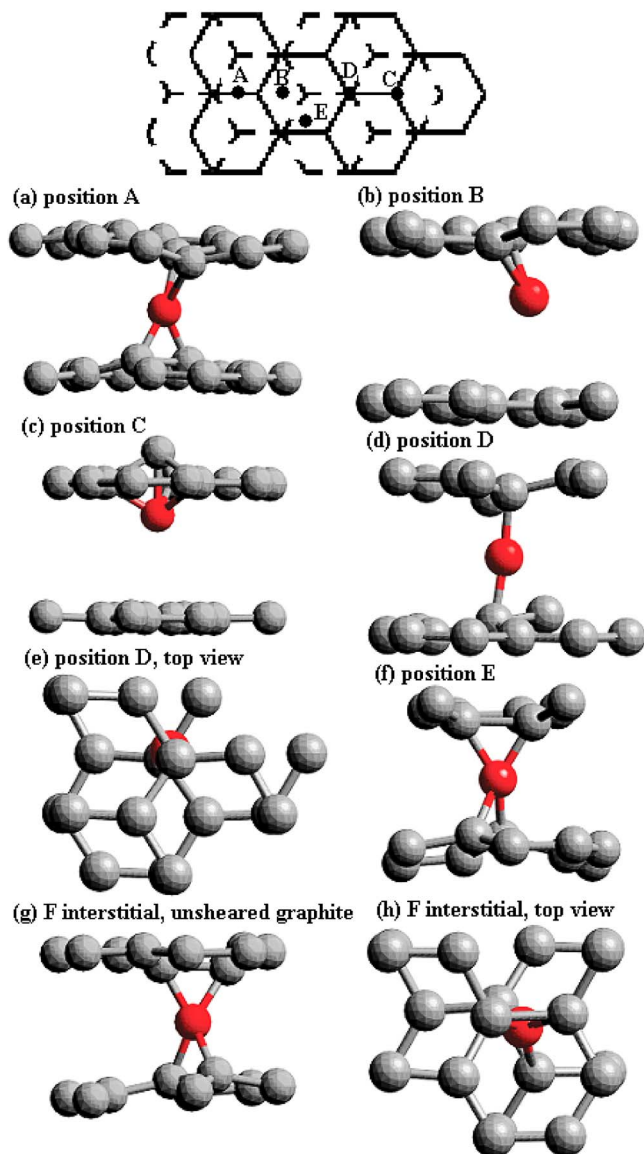


FIG. 2. (Color online) Configurations of the interstitials at the various sites *A* to *E* and for the free (*F*) interstitial as obtained with CASTEP and GGA; compare Table II. Light gray atoms are part of graphite; the interstitial is shown in dark gray (red). For the high-symmetry positions *D* and the free interstitial the top view is given as well. The inset at the top shows the high symmetry sites for an interstitial in graphite.

and a long bond of 1.7 \AA to a second neighbor atom. After relaxing the atoms in the graphene layer, the formation energy decreases by 0.5 eV to $\approx 7.2 \text{ eV}$; see Table I. Finally, in position *C* above the center of a hexagon, the adatom does not make bonds to layer atoms, and this is the most unstable position with a formation energy of more than 8 eV . The adatom lies 1.66 \AA above the graphite plane, at 2.15 \AA from the atoms [Fig. 2(c)].

The formation energies of an adatom thus depends on the number of bonds the adatoms form with the carbon atoms in the layer. The formation energies are smallest ($\approx 6.7 \text{ eV}$) for adatoms that have two bonds to the graphene layer (sites *A*, *B*, and *E*). Site *D* has two bonds with different lengths in the

relaxed structure. Moreover, an adatom at *D* strongly strains the graphene sheet, which makes the configuration less stable. Site *C* has the largest formation energy, because no bond forms between the adatom and graphene.

The energy of a carbon atom well away from the layers is 9.4 eV in a spin-restricted calculation. This reduces to 8.3 eV for a spin-polarized calculation, as the isolated carbon atom is in a triplet configuration. This implies an absorption energy of 1.7 eV for the *A* site. These values compare to an adsorption energy of 1.4 eV at the *A* site found in the spin-unrestricted LDA calculations of Lehtinen *et al.*¹⁵ and 1.78 eV in the local-orbital LDA calculations of Lee *et al.*¹⁷ They found a smaller energy difference (0.18 eV) between the bridged and on-top sites than we did, but the order between sites *A*, *D*, and *C* was the same.

V. SIMPLE INTERSTITIALS

We now consider interstitials in bulk graphite. The high-symmetry sites of interstitials are labeled as for the adatom in Fig. 2. Site *A* is the bridge site above a bond center, site *C* is above an atom in one layer and above a hexagon center in the other layer, while site *D* is directly between an atom in both adjacent layers. Table III gives the formation energies of the interstitial at the different sites.

We first compare the formation energies obtained with the GGA and the LDA, CASTEP and SIESTA, and smaller and larger supercells. The formation energies using the GGA are systematically by 5% ($\approx 0.3 \text{ eV}$ root mean square) larger than the energies within the LDA. This is of similar magnitude as the ratio between the cohesive energies in the spin-restricted calculations; see Tables I and II. Similarly, the SIESTA results within the LDA are smaller than within CASTEP by 7% ($\approx 0.4 \text{ eV}$ root mean square). These deviations originate from two sources, the difference in energy gain by carbon-carbon bonds (Table I) and the optimization of the atomic positions. The latter was more restrictive in CASTEP (four atoms fixed in all three directions) than in SIESTA (constraints only in the *ab* plane). Nevertheless, the differences between the formation energies found with CASTEP and SIESTA are again systematic. The order of the high-symmetry sites is the same and the maximum difference in formation energy between two high-symmetry positions is very similar.

The last two rows in Table III show the convergence of the formation energies with the size of the supercell. We compare the energies found for 3×3 supercell with three layers and a 4×4 supercell with four layers using SIESTA and a DZ basis. As can be seen in Table II, the deviations are at most 2.5% . The error introduced by the size of the supercell is thus smaller than the uncertainties resulting from the exchange-correlation functional and the size and type of the basis set. All these uncertainties are smaller than the difference in formation energy we obtain for interstitials in different high-symmetry positions.

The formation energies in Table III depend strongly on the position of an interstitial atom. E_f is correlated with the number of bonds an interstitial forms with the carbon atoms in the layer. The most stable, high-symmetry site [smallest

TABLE III. Formation energies with the GGA and the LDA using CASTEP and SIESTA of simple interstitials in different configurations, compare Fig. 2. The last two rows verify the convergence with the size of the supercell using a DZ basis set, see Sec. II A. All formation energies are in eV.

Site	A Spiro	B Bridge	C On top	D	E Spiro	F Free
GGA, CASTEP, 55 atoms						
	6.8	8	7.8	8	6.5	6.3
LDA, 55 atoms						
PW, CASTEP	6.5	7.8	7.3	7.7	6.2	5.9
DZP, SIESTA	6.1	7.7	6.7	7.4	5.8	5.5
LDA, DZ, SIESTA						
55 atoms	6.8	8.5	8	8	6.5	6.1
129 atoms	6.9	8.4		8.2		

E_f , see Eq. (1)] is site *E* in Table III regardless of the details of the calculation. At this site, the interstitial forms four bonds, of length 1.48 Å and 1.53 Å, two to each layer, as in Fig. 2(f). The next stable high-symmetry site is site *A*. Here, as in Fig. 2(a), the interstitial sits away from the center of the interlayer and it forms two bonds to one layer of lengths 1.5 Å and 1.6 Å, and two bonds to the other layer both of 1.5 Å. Allowing the *E* interstitial to relax in all three directions, we obtain the site with the lowest formation energy in unsheared graphite, denoted *F* or free (Table III). The *F* interstitial makes two bonds with a length of 1.48 and 1.52 Å to the layer above and below the interstitial, respectively; see Fig. 2(g). Within the *ab* plane the relaxed interstitial is close to the high-symmetry site *E*, but moved slightly out of the center of the triangular towards the *D* position, as can be seen in Fig. 2(h).

The *F* interstitial in unsheared graphite and the *A* and *E* high-symmetry sites all have a formation energy below 7 eV; see Table III. In these three configurations, the interstitial forms four bonds of similar length ≈ 1.5 Å. Site *C* is the next high-symmetry site in order of increasing formation energy with $E_f=6.7-7.3$ eV depending on the exchange-correlation functional and the type of the basis set. In this site the interstitial moves towards the carbon atom above it and pushed this atom out of the graphite layer; see Fig. 2(c). The interstitial forms three bonds with length 1.56 Å; the angles between the interstitial-layer-atom bonds are 97°.

Sites *B* and *D* have the highest formation energies of all high-symmetry positions. In both sites the interstitial forms only two strong bonds. In site *B*, Fig. 2(b), the added atoms binds to its nearest neighbors in one layer with bond lengths of 1.52 and 1.62 Å. In site *D* the interstitial has two bonds of length 1.44 Å to the atoms above and below; the distance to two of its second neighbors decreased from 2.2 Å to (1.75 ± 0.05) Å; see Fig. 2(d). In site *D* the graphite layers above and below the interstitial are strongly strained. The two carbon atoms directly above and below the interstitial moved out of their high-symmetry positions in the *ab* plane; see Fig. 2(e). The angle between the two short bonds between the interstitial and its two neighbors thereby decreased from 180° to 165°.

The formation energies depend closely on the numbers of bonds formed by the interstitial. Sites *E* and *A* form four

bonds, two to the layer above and two to the layer below the interstitial. This configuration has been called a *spiro* by Telling *et al.*,¹¹ so-called because of its resemblance to the core of the molecule spiro-pentane. The lowest energy interstitial configuration of high symmetry is *E* and the diffusion path passes over site *B*. This corresponds to a migration energy of more than 1.5 eV (>1.7 eV when referred to the fully relaxed position, in Table III). This is much larger than the experimental value of 0.1 eV.

The most notable feature of these formation energies is that they span a much larger range than those of previous calculations such as Xu *et al.*⁷ They also appear to contradict the experimental values of Thrower and Mayer,¹ particularly the notably low migration energy of 0.1 eV. Our values, however, agree broadly with values found by El-Barbary *et al.*³³ Heggie^{33,34} suggests that the experimental formation energies of Thrower and Meyer¹ correspond to a simplified interpretation of defect migration, which does not include more complex forms of disorder such as shear.³⁵

VI. SHEARED INTERSTITIALS

The low formation energy of the configurations *A*, *E*, and *F* in unsheared graphite described above already suggests that the lowest energy interstitial site has a low symmetry. It is well known that the shear energy of graphite layers is very small, because of the weak interlayer bonding.³⁶ The interesting result found by Telling *et al.*¹¹ is that the interlayer interstitials are stabilized if a graphite layer is allowed to shear with respect to the adjacent layers. The shear allows the interstitial atom to bond to more atoms in adjacent layers than for the simple interstitial. It will also attract the layers slightly to do this.

The shear energy is proportional to the layer area which is displaced. Thus, an interesting point is that increasing the lateral size of the supercell does not necessarily help convergence, as the total energy of the cell can appear to increase. In fact, large cells starting with the ideal structure have difficulty finding the minimum energy configuration, and the shear should be included in the starting structure to overcome this.

For the calculations of shear graphite, we started from the following relaxed configurations of unsheared graphite, the

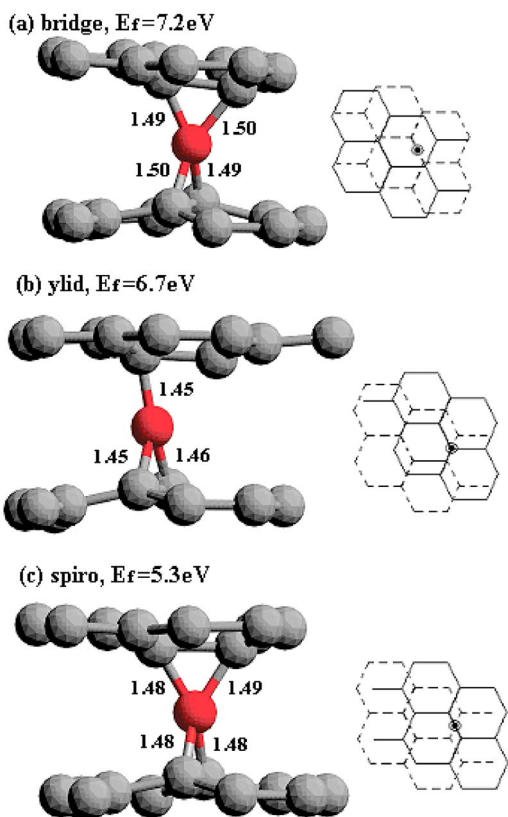


FIG. 3. (Color online) Three interstitial structures in sheared graphite: (a) bridge, (b) ylid, and (c) spiro (compare Table III). The interstitial atom is shown in dark gray (red); graphite is shown in light gray. All the bond lengths are in Å. The right panels in (a)–(c) show schematically the shear induced by the interstitial. The formation energies were obtained with CASTEP and the GGA, compare Sec. II A.

fully relaxed geometry (free), sites *B* and *D*. In the first two starting configurations we allowed all carbon atoms to relax, obtaining the global and a local minimum configuration. For site *D* we allowed the atoms except one corner atom and the interstitial to relax. This resulted in a ylid position with three bonds, which is further discussed below.

Three new geometries were found, depending on the size and direction of the shear. The simplest is the bridged inter-

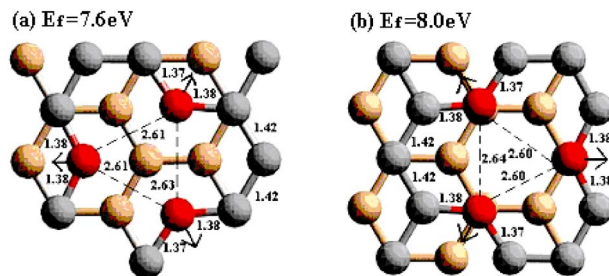


FIG. 4. (Color online) Two types of vacancies: (a) V_α and (b) V_β . Arrows indicate relaxation directions for the nearest neighbors (red) of a V . The layer below is light brown. All bond lengths are in Å.

stitial, which corresponds to site *B* in unsheared graphite. The shear is $0.1a_{CC}$, $[110]$ where $a_{CC}=a_0/\sqrt{3}=1.41$ Å is the bulk bond length. The sheared cell is schematically shown in the right side of Fig. 3(a). The interstitial makes four bonds with the layers above and below. The bond lengths are 1.50 Å in this configuration, about 5% larger than in bulk graphite; see Fig. 3(a).

The second configuration for a shear is half a bond length in a bond direction or $1/2a_{CC}$, $[110]$; compare right panel in Fig. 3(b). This shear allows the formation of the ylid interstitial (starting from the *D* site of unsheared graphite) with $E_f=6.7$ eV. The ylid is so called because of the *y* arrangement of bonds around the interstitial, two bonds to one layer and one bond to the opposite layer within a vertical plane. The bond lengths in this case are 1.45 Å. The strong bonds to both layers have caused the layers to move together around the interstitial; see Fig. 3(b).

The third configuration occurs for a shear of $1/2a_{CC}$ $[100]$, shown in the right panel in Fig. 3(c). The interstitial then forms a so-called spiro configuration in which it forms four bonds, two to each layer. This site is the most stable of the interstitials, having a formation energy of only 5.3 eV. This energy is nearly 1 eV below that of the most stable simple interstitial; compare the GGA results in Table II and III. In this case, the bond lengths are 1.48 Å as shown in Fig. 3(c). Again, the graphite layers have been brought together to achieve these shorter lengths. The last two configurations have cross links between neighboring graphite sheets.

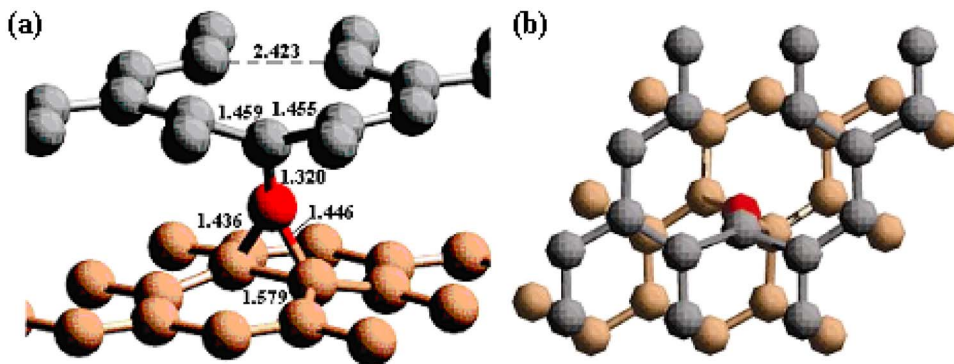


FIG. 5. (Color online) The intimate I-V pair in sheared graphite (a) side view (b) top view. The interstitial atom is red; atoms in the sheet below are light brown. All bond lengths are in Å. Dashed line indicates the weakly reconstructed vacancy bond.

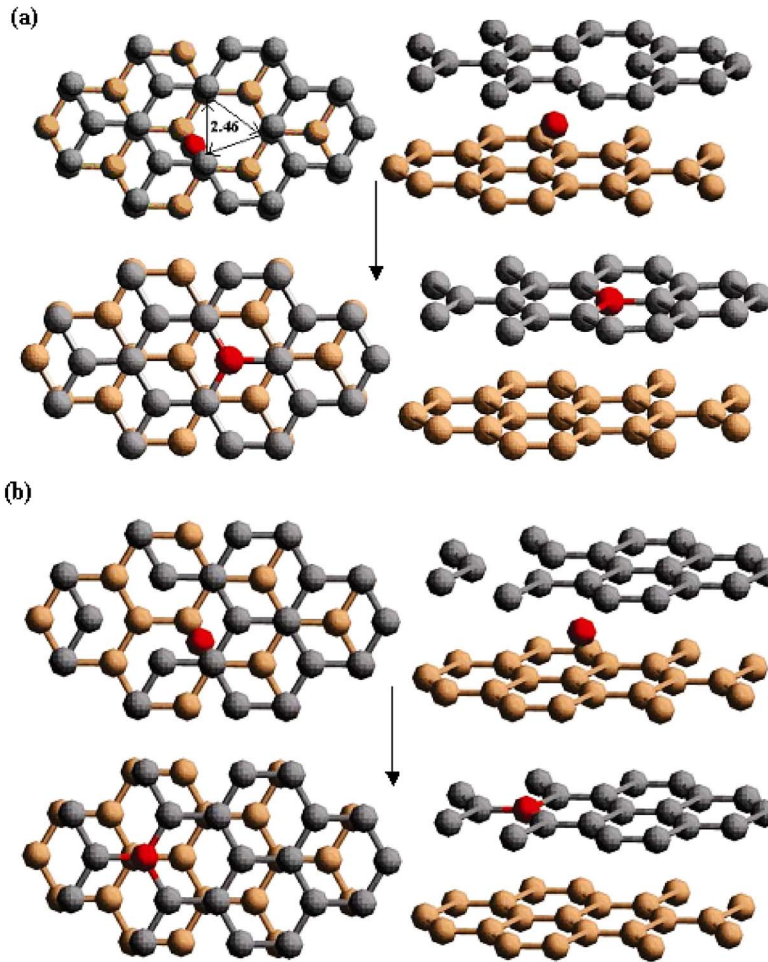


FIG. 6. (Color online) The recombination process between an interstitial and a vacancy in unsheared graphite; (a) I and V_β and (b) I and V_α . All bond lengths are in Å.

The interstitials of shear graphite lower their energy by segregating at the dislocation core. Comparing with the cross links in the perfect graphite, they are much more stable in the dislocated graphite. Nevertheless, the energy differences between the lowest-energy, spiro configuration and the less stable bridge and ylid configuration are similar to unsheared graphite, $\Delta E_f(\text{sheared}) \geq 1.4$ eV, and $\Delta E_f(\text{unsheared}) \geq 1.5$ eV.

VII. VACANCIES

The AB plane structure of hexagonal graphite allows there to be two vacancy structures. Vacancy V_α consists of a vacancy lying directly above an atom site on the adjacent layers. Its formation energy is calculated to be 7.6 eV in GGA. The other configuration V_β is a vacancy site lying between centers of hexagonal voids on the planes adjacent to the plane of the vacancy. Its formation energy is found to be 8 eV. Our values compare to 7.8 eV found by Kaxiras and Pandey⁹ and 7.4 eV by Al-Barbary *et al.*³³ The vacancy atomic configurations and the directions of atomic relaxation are shown in Fig. 4. The three nearest atoms move away from the vacancy and are displaced by about 0.4 Å. The displacement of the more distant atoms is, however, sufficiently smaller. This result contrasts with the results of Xu,⁷ where the vacancy's first neighbors move closer to the va-

cancy and the first and second neighbors are displaced by 0.3 Å. The migration barrier for vacancies is an order of magnitude larger than that of the interlayer interstitials.⁹

VIII. INTERSTITIAL-VACANCY (I-V) PAIR

The various configurations of interstitial sites allows the possibility of a variety of interstitial-vacancy configurations. In many materials, a nearby vacancy and interstitial will recombine to give a perfect lattice without any energy barrier. In other cases, they can form an I-V bound pair. Ewels *et al.*¹² found that both possibilities can occur in graphite, depending on the symmetry of the interstitial atom. Their calculations used a local-orbital basis and the LDA. Our calculations using a plane-wave basis and GGA find that the structure adopted depends on whether the interstitial initially lies in a sheared or unsheared graphite.

A vacancy site, V_α and V_β , is introduced, and an interstitial atom is placed at various sites around it in a sheared graphite. The interstitial and the vacancy interact to form a metastable I-V complex, referred to as an intimate I-V pair. Its formation energy is calculated to be 10.8 eV. This is a gain in energy of 2.1 eV compared to the most stable isolated interstitial and vacancy configurations, even in sheared graphite. In the most stable form of this complex, the interstitial adopts the ylid structure. The plane of the vacancy is sheared

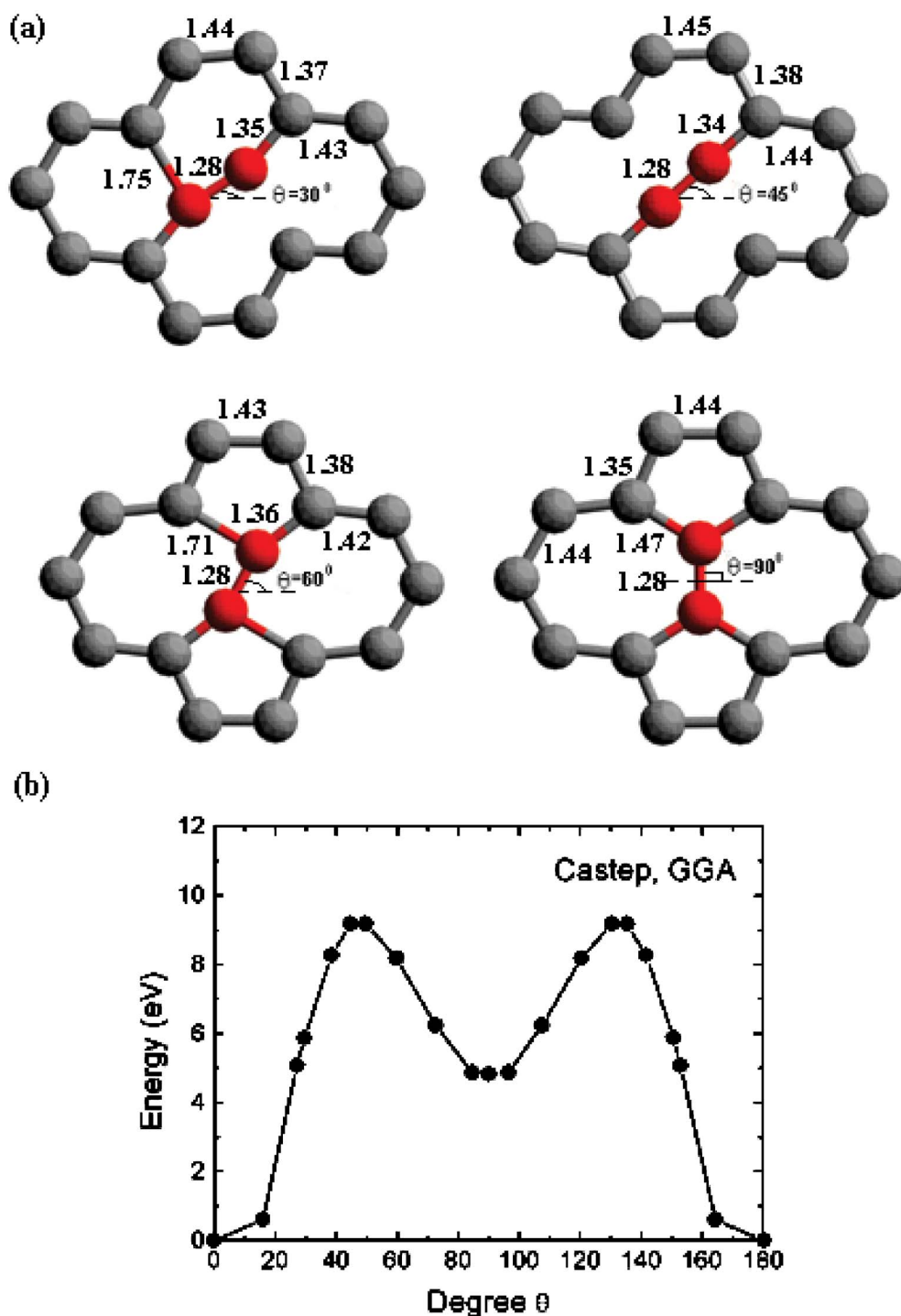


FIG. 7. (Color online) Stone-Wales defect. (a) In-plane atom pair exchange within the GGA for different θ as indicated in the panels. The direct-exchange atoms are dark gray (red). All the bond lengths are in Å. (b) The corresponding formation energy as a function of the rotation angle θ .

by $1/2a_{CC}$ [110] with respect to the adjacent layers, as in the isolated ylid interstitial (Fig. 5). The interstitial atom is bonded to one of the three C atoms surrounding the vacancy and also bonds to two C atoms in the sheet below. The two other C atoms around the vacancy form a weakly reconstructed bond. The single bond from the interstitial to the vacancy is extremely short, 1.32 Å, while the other two are 1.44 Å. The short bond is a distorted double bond, which

accounts for the stability of this I-V complex. This complex can only recombine into perfect graphite once the recombination barrier of about 1.3 eV is overcome.¹¹

In unsheared graphite, the interstitial sites are less stabilized. This allows the I-V pairs to recombine without a barrier. In this case, we find that the recombination process is barrierless, whatever the type of vacancy, V_α and V_β , the form of interstitial, or the distance between the vacancy and

the interstitial are, as shown in Fig. 6. As described in the previous section, the cross-linked structures for interstitials are unstable in unsheared graphite. Therefore, during geometry optimization the I-V defect would relax to the perfect graphite associated with lower energy.

IX. STONE-WALES DEFECTS

The Stone-Wales (SW) transformation in a graphite sheet is the rotation of a pair of atoms by 90° to convert four hexagonal rings into two pentagons and two heptagons, as in Figs. 7(a) and 7(b). The pair of five- and sevenfold rings is a dislocation dipole with an in-plane Burgers vector, so a Stone-Wales defect is also two back-to-back dislocation cores.

Figure 7(d) shows the energy as a function of rotation angle of the atom pair in the defect. The SW defect is found to have a formation energy of 4.8 eV within the GGA; see Fig. 7(b). However, there is also a substantial energy barrier to its formation or removal. The top of the barrier is 9.2 eV above the perfect lattice or 4.4 eV above the SW defect level. The transition state at the top of the barrier is roughly at a rotation angle of 45° and corresponds to the structure shown for $\theta=45^\circ$ in Fig. 7(a). The large barrier energy is due to the large atom rearrangements needed, including the breaking of two C—C bonds at the transition state.

In the SW defect, the two central atoms get closer to each other by 5% of the interatomic distance. The displacements of the other atoms are 3% in the first neighbors, 2.5% in the second neighbors, 1.5% in the third neighbors, and less than 1% in the farther neighbors. Our results are different from Xu *et al.*'s⁷ suggestion that the displacements of atoms up to the fifth nearest neighbors are very significant.

Our calculated SW energies of 4.8 eV within the GGA and 5.2 eV within LDA are lower than the Huckel value of 6.02 eV of Zhou and Shi²⁴ and 5.9 eV for graphite found by Jensen *et al.*²² by SIESTA. The latter was obtained with a DZ basis set. In view of the differences in formation energy be-

tween plane-wave and DZ local-orbital calculations discussed in Sec. IV (compare Table III), there is reasonable agreement between Jensen *et al.*'s²² and our SW energies. The SW defect energy is much less than the “concerted exchange” energy of over 10 eV found by Kaxiras and Pandey⁹ because they did not include relaxation of the neighboring atoms.

The barrier height of 9.2 eV (9.4 eV within the LDA) compares well with the 10 eV barrier found by local-orbital DFT calculations.²³ In nanotubes, the SW barrier energy is of great interest because it decreases as a function of strain and curvature.²⁰ Plastic flow and fracture is believed to occur via the SW mechanism.

X. CONCLUSIONS

This paper has investigated the energetics of interstitials, vacancies, I-V pairs, and the Stone-Wales defects. It has been found that the defects, whether they are in-plane or out-of-plane, have high formation energies on the carbon materials (graphite, carbon nanotubes, fullerenes, etc.). A barrier for interstitials to diffuse exists. On a single layer of graphite, the interstitial prefers to form a bridge configuration. In graphite, the interstitial prefers to shear graphite layers to form the bridge, the ylid, or the spiro configuration. The spiro structure is the most stable. The energy barrier to metastable configurations is at least 1.4 eV. In sheared graphite, an I-V pair would relax into an intimate I-V pair with lower formation energy. The ylid interstitial neighboring the vacancy is favored. On the other hand, in unsheared graphite, an interstitial will recombine with a vacancy to form perfect graphite without any barrier.

ACKNOWLEDGMENTS

The authors thank the EC project CARDECOM for partial funding. S. R. was supported by the Oppenheimer Trust and Newnham College.

*Electronic address: ll260@eng.cam.ac.uk

†Present address: Department of Materials Science and Engineering, MIT, Cambridge, Massachusetts 02139.

¹P. A. Throver and R. M. Mayer, *Phys. Status Solidi A* **47**, 11 (1978).

²C. A. Coulson, M. A. Herraes, M. Leal, E. Santos, and S. Senent, *Proc. R. Soc. London, Ser. A* **274**, 461 (1963).

³C. A. Coulson and M. D. Poole, *Carbon* **2**, 275 (1964).

⁴A. P. P. Nicholson and D. J. Bacon, *Carbon* **13**, 275 (1975).

⁵A. Zunger and R. Engelman, *Phys. Rev. B* **17**, 642 (1978).

⁶C. Pisani, R. Dovesi, and P. Carosso, *Phys. Rev. B* **20**, 5345 (1979).

⁷C. H. Xu, C. L. Fu, and D. F. Pedraza, *Phys. Rev. B* **48**, 13273 (1993).

⁸E. Kaxiras and K. C. Pandey, *Phys. Rev. Lett.* **61**, 2693 (1998).

⁹M. I. Heggie, B. R. Eggen, C. P. Ewels, P. Leary, S. Ali, G. Jungnickel, R. Jones, and P. R. Briddon, *Proc.-Electrochem.*

Soc. **98-8**, 60 (1997).

¹⁰R. H. Telling, C. P. Ewels, Ahlam A. El-Barbary, and M. I. Heggie, *Nat. Mater.* **2**, 333 (2003).

¹¹C. P. Ewels, R. H. Telling, A. A. El-Barbary, and M. I. Heggie, *Phys. Rev. Lett.* **91**, 025505 (2002).

¹²A. Hashimoto, K. Suenaga, A. Gloter, and K. Urita, *Nature* **430**, 870 (2004).

¹³K. Urita, K. Suenaga, T. Sugai, H. Shinohara, and S. Ijima, *Phys. Rev. Lett.* **94**, 155502 (2005).

¹⁴P. O. Lehtinen, A. S. Foster, A. Ayuela, A. Krashennikov, K. Nordlund, and R. M. Nieminen, *Phys. Rev. Lett.* **91**, 017202 (2003).

¹⁵K. Nordlund, J. Keinonen, and T. Mattila, *Phys. Rev. Lett.* **77**, 699 (1996).

¹⁶Y. H. Lee, S. G. Kim, and D. Tomanek, *Phys. Rev. Lett.* **78**, 2393 (1997).

¹⁷F. Banhart, *Rep. Prog. Phys.* **62**, 1181 (1999).

- ¹⁸A. J. Stone and D. J. Wales, Chem. Phys. Lett. **128**, 501 (1986).
- ¹⁹B. R. Eggen, M. I. Heggie, G. Jungnickel, C. Latham, R. Jones, and B. R. Briddon, Science **272**, 87 (1996); C. P. Ewels, M. I. Heggie, and P. R. Briddon, Chem. Phys. Lett. **351**, 178 (2002).
- ²⁰M. B. Nardelli, B. I. Yakobson, and J. Bernholc, Phys. Rev. Lett. **81**, 4656 (1998).
- ²¹G. G. Samsonidze, G. G. Samsonidze, and B. I. Yakobson, Phys. Rev. Lett. **88**, 065501 (2002).
- ²²P. Jensen, J. Gale, and X. Blase, Phys. Rev. B **66**, 193403 (2002).
- ²³T. Dumitrica and B. I. Yakobson, Appl. Phys. Lett. **84**, 2775 (2004).
- ²⁴L. G. Zhou and S. Q. Shi, Appl. Phys. Lett. **83**, 1222 (2004).
- ²⁵V. Milman, B. Winkler, J. A. White, C. J. Pickard, and M. C. Payne, Int. J. Quantum Chem. **77**, 895 (2000).
- ²⁶J. M. Soler *et al.*, J. Phys.: Condens. Matter **14**, 2745 (2002).
- ²⁷D. Vanderbilt, Phys. Rev. B **41**, 7892 (1990).
- ²⁸N. Troullier, and J. L. Martins, Phys. Rev. B **43**, 1993 (1991).
- ²⁹J. Junquera, O. Paz, D. Sánchez-Portal, and E. Artacho, Phys. Rev. B **64**, 235111 (2001).
- ³⁰C. Van de Walle and J. Neugebauer, J. Appl. Phys. **95**, 3851 (2004).
- ³¹J. Furthmüller, J. Hafner, and G. Kresse, Phys. Rev. B **50**, 15606 (1994); G. Kern, Ph.D. thesis, TU Wein, 1997.
- ³²J. C. Boettger, Phys. Rev. B **55**, 11202 (1997).
- ³³A. A. El-Barbary, R. H. Telling, C. P. Ewels, M. I. Heggie, P. R. Briddon, Phys. Rev. B **68**, 144107 (2003).
- ³⁴M. I. Heggie (private communication).
- ³⁵K. Niwase, Philos. Mag. Lett. **82**, 401 (2002).
- ³⁶R. H. Telling and M. I. Heggie, Philos. Mag. Lett. **83**, 11 (2003).